Comparative Analysis of Departure Metering at United States and European Airports

Sandeep Badrinath, Hamsa Balakrishnan, Ji Ma, Daniel Delahaye

Comparative Analysis of Departure Metering at United States and European Airports

Sandeep Badrinath * and Hamsa Balakrishnan[†]

Department of Aeronautics and Astronautics, Massachusetts Institute of Technology, Cambridge, MA-02139

Ji Ma [‡] and Daniel Delahaye[§]

ENAC, Université de Toulouse, 31400 Toulouse, France

Departure metering has the potential to mitigate airport surface congestion and decrease flight delays. This paper considers several candidate departure metering techniques, including a trajectory-based optimization approach using a node-link model and three aggregate queue-based approaches (a scheduler meant to represent NASA's Airspace Technology Demonstration-2 (ATD-2) logic, an optimal control approach, and a robust control approach). The outcomes of these different approaches are compared for two major airports: Paris Charles De Gaulle airport (CDG) in Europe and Charlotte Douglas International airport (CLT) in the United States. These two airports have similar aggregate demand and capacity, but the banking of demand at CLT leads to congestion, resulting in higher taxi-out delays and more potential for departure metering at CLT. Stochastic simulations are used to show that departure metering with the robust control approach best accommodates operational uncertainties, and that departure metering yields higher taxi-out time savings at CLT compared to CDG, irrespective of the approach.

Nomenclature

Δt =   Time step

Δv =   Speed increment

s =   Minimum taxi separation distance

$V^{\min}$ =   Minimum allowed taxi speed

$V^{\max}$ =   Maximum allowed taxi speed

$N\Delta t$ =   Maximum allowed holding time, N^a for arrivals and N^d for departures

$N_p\Delta t$ =   Maximum allowed pushback delay

---

*PhD candidate, Department of Aeronautics and Astronautics. AIAA Student Member.
[†]Professor, Department of Aeronautics and Astronautics. AIAA Associate Fellow.
[‡]PhD candidate, ENAC, also SIAE, CAUC, Tianjin 300300, China.
[§]Professor, ENAC, Université de Toulouse.

$\mathcal{F}$	=	Flight set, $\mathcal{F} = \mathcal{A} \bigcup \mathcal{D}$, $\mathcal{A}$ for arrivals and $\mathcal{D}$ for departures
G_f	=	Gate number of flight f
r_f	=	Landing or take-off runway of flight f
I_f	=	Initial off-block time or initial landing time of flight f
h_f	=	Holding point of flight f
γ_f	=	Taxi route of flight f
p_f	=	Pushback time of flight f
w_f	=	Holding time of flight f
v_f	=	Taxi speed of flight f
t_f^u	=	Runway usage time of flight f
t_f^c	=	Completion time of flight f
t_f^n	=	Passage time of flight f at node n
$t_{f,n}^{\text{In}}$	=	Entry time of flight f to the detection zone of node n
$t_{f,n}^{\text{Out}}$	=	Exit time of flight f from the detection zone of node n
s_{fg}	=	Minimum runway separation time between two consecutive flights f and g
Φ_p	=	Average pushback delay
Φ_d	=	Average taxi-out time
Φ_a	=	Average taxi-in time
$\lambda(t)$	=	Mean in-flow rate into the queue
$\mu(t)$	=	Mean service rate of the server
$x(t)$	=	Dynamics of the queue length
τ_{gr_i}	=	Average unimpeded travel time from the gate to the ith departure runway
u_{d_i}	=	Pushback rate to the ith departure runway
x_{s_i}	=	Number of aircraft in the ramp queue that are bound for the ith departure runway
τ_{gs}	=	Average unimpeded travel time from the gate to the spot
τ_{si}	=	Average unimpeded travel time from the spot to the ith runway
Y	=	Excess queue time buffer for the rule-based heuristic
T	=	Time horizon over which the cost is minimized in the optimal control approach
T_p	=	Planning horizon

I. Introduction

Surface congestion results in excessive taxi times and delays at major airports around the world [1]. Departure metering, in which departures are appropriately held at the gate in order to reduce taxi-out time, while ensuring no adverse impact on the airport throughput, has been shown to be an effective congestion management technique [2–4]. An aircraft saves fuel while waiting at the gate with its engines off compared to idling in a taxi queue with its engines on. Departure metering is estimated to provide $5.5-9.5 billion in monetary benefits at the top 35 airports in the US over a 20-year period [5], and is an integral part of airport surface management programs internationally [6–9].

Departure metering solutions can be broadly classified into aircraft-specific trajectory-based approaches and aggregate queue-based approaches. A trajectory-based approach uses a detailed node-link network model for the airport surface, and determines an optimal four-dimensional (4D) taxi trajectory for each aircraft, accounting for potential conflicts with other flights [10]. The resulting large-scale optimization problems have been solved using a range of computational methods [11–16]. By contrast, a queue-based approach determines an aggregate pushback rate at any time, considering macroscopic factors such as surface queue lengths or average taxi-out times, which are determined using low-fidelity queuing models [17–19].

In this paper, we present a comparative analysis of four departure metering techniques applied to two major airports: Paris Charles De Gaulle Airport (CDG) and Charlotte Douglas International Airport (CLT). The first of these techniques is trajectory-based optimization, while the other three are queue-based approaches. One of them reflects NASA's Airspace Technology Demonstration-2 (ATD-2) logic, which has been field-tested at CLT since November 2017 [2]. Two other queue-based approaches, an optimal control approach [19] and a new robust control approach that explicitly handles model uncertainties are also analyzed, using models of the two airports developed and validated using operational data.

The main contributions of this paper are as follows: We describe two data-driven techniques for modeling the airport surface: the first based on a node-link model, and the second based on a queuing network. We adapt these models to both CLT and CDG. These models are used to develop departure metering algorithms that regulate the pushback of aircraft from their gates during periods of congestion. The node-link models are used for trajectory-based optimization, whereas the queuing network based models are used to adapt the ATD-2 logic as well as develop optimal and robust control policies. The impacts of the different departure metering algorithms are then evaluated using stochastic simulations of operations at CLT and CDG, in order to gain insights on the effectiveness of the different approaches, as well as the influence of airport layout and departure demand profiles.

II. Modeling of airport surface operations

The comparison of benefits with different departure metering approaches across airports requires the modeling of airport surface operations. This paper uses models that were built and validated with data that included flight tracks,

the actual pushback, in-air (wheels-off), landing (wheels-on) and in-gate times, gate assignments, and meteorological conditions at the airports [21–23]. In particular, the data corresponded to CLT operations in May-July 2015 and May-June 2016, and CDG in July-August 2017. The periods of data were chosen based on availability, and to include periods of high demand.

A. Overview of CDG operations

CDG is the 2nd busiest airport in Europe and the 11th busiest airport in the world in terms of aircraft movements, with 1,300 flights/day and 66 million passengers in 2016 [24]. The airport has four parallel runways, and operates under two broad runway configurations: West-flow ($26L, 27R|26R, 27L$) and East-flow ($09L, 08R|09R, 08L$). This paper focuses on the more frequently-used West-flow configuration (75% of operations in July-August 2017). Fig. 1(a) shows the CDG layout along with a snapshot of the traffic in the West-flow configuration. Departing flights are represented by black triangles and arriving flights represented by white ones. The departure and arrival runways are indicated using blue and red arrows, respectively. We note the queues of aircraft near the departure runways.

B. Overview of CLT operations

CLT is the 7th busiest airport in the world in terms of aircraft movements, with 1,400 flights/day and 44.4 million passengers in 2016 [23, 24]. It has three parallel runways and one intersecting runway, and operates under two broad runway configurations: North-flow (36C, 36L, 36R | 36C, 36R) and South-Flow (18L, 18C, 18R, 23 | 18C, 18L). We focus on the North-flow configuration which handled about 52% of the traffic during 2015-2016 [22]. Fig. 1(b) shows the airport layout of CLT. The leftmost runway (36L) is used only for arrivals, whereas runways 36C and 36R are used for mixed operations. CLT experiences congestion at multiple locations, resulting in the formation of queues in the ramp area and near the runway crossing, in addition to the departure runway queues.

(a) CDG in West-flow runway configuration. (b) CLT in North-flow runway configuration [20].
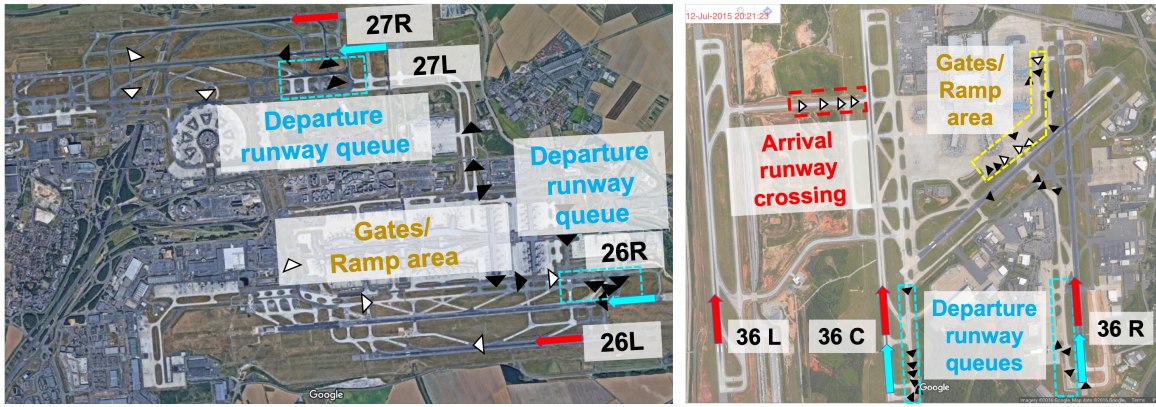
Fig. 1   Airport layout with a snapshot of traffic movement.

C. Comparison of CDG and CLT

Although the two airports handle approximately the same number of aircraft movements, their fleet mixes are significantly different, with CDG handling a larger percentage of 'heavy' aircraft (25%) compared to CLT (2%). CDG operates under instrument meteorological conditions (IMC) capacity even in visual conditions, unlike CLT. Both airports have the same number of departure runways, but CLT has mixed operations. Consequently, the declared departure capacities in good weather conditions are similar at both airports. Another differentiating feature is the nature of demand. Figure 2 shows the number of pushbacks (per 15 mins), declared departure capacity and total runway queue length for a typical day at the two airports. The total runway queue length corresponds to a time-based definition of queue length, in which an aircraft is said to be in the runway queue if it has spent unimpeded gate-to-runway time after pushback but is yet to take-off. Our analysis has found that this time-based definition is consistent with the observed physical queue. The figure (Fig. 2) shows that the departure demand is significantly banked at CLT compared to CDG, resulting in periods of higher demand-capacity imbalance, leading to the formation of larger queues. One can also notice that the demand at CDG rarely exceeds capacity since it is slot-coordinated, unlike CLT. The higher imbalance between demand and capacity at CLT leads to higher taxi-out delays. The average taxi-out delay is 4.2 min at CDG and 9 min at CLT. We would therefore expect higher benefits from departure metering at CLT.

III. Trajectory-based optimization

In the trajectory-based approach, the airport surface is represented as a node-link network. (Figs. 3(a) and 3(b)). Nodes correspond to runway entry/exit points, holding points, and intersections of taxiways or gates. A holding point refers to the runway threshold for departures and runway crossing point for arrivals. Links connect two adjacent nodes. The links corresponding to the pushback area, ramp area and active movement area are indicated in Fig. 3 using green, red and blue, respectively. The modified pushback times for departure metering are determined as a solution to an optimization problem, as described below.

A. Problem formulation

1. Inputs

The inputs to the optimization problem are a set of runways ($\mathcal{R}$); a set of holding points ($\mathcal{H}$); time-step (Δt); maximum allowed holding time ($N\Delta t$), denoted by N^a for arrivals and N^d for departures; maximum allowed pushback delay ($N_p \Delta t$); maximum capacity at holding points (C), denoted by C^a for arrivals and C^d for departures; speed increment (Δv); minimum taxi separation distance (s); minimum allowed taxi speed ($V^{\min}$); maximum allowed taxi speed ($V^{\max}$); the set of flights ($\mathcal{F} = \mathcal{A} \bigcup \mathcal{D}$, $\mathcal{A}$ for arrivals and $\mathcal{D}$ for departures). For all flights $f \in \mathcal{F}$: gate number (G_f); landing or take-off runway ($r_f \in \mathcal{R}$); initial off-block time for departures or initial landing time for arrivals (I_f); holding point ($h_f \in \mathcal{H}$); taxi route (γ_f) containing a set of nodes (including gate, runway, holding point, and intersection

(a) CDG (July 10th, 2017)
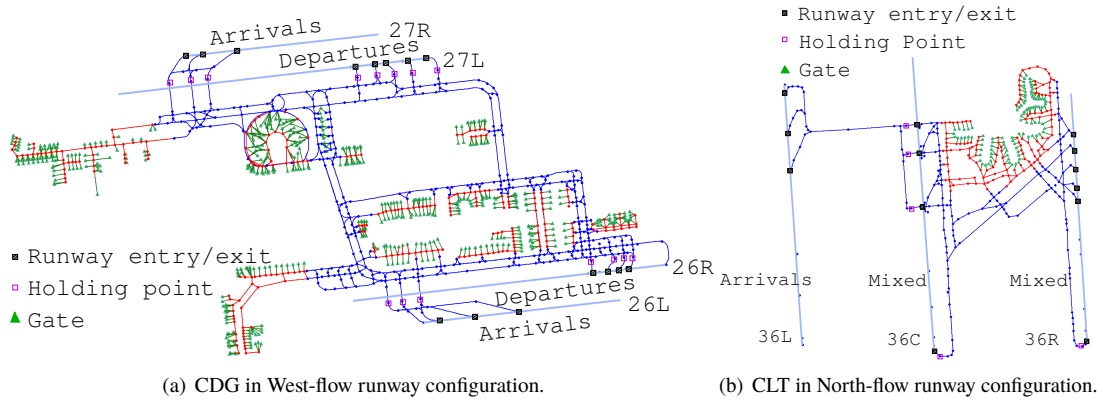

(b) CLT (May 7th, 2015)
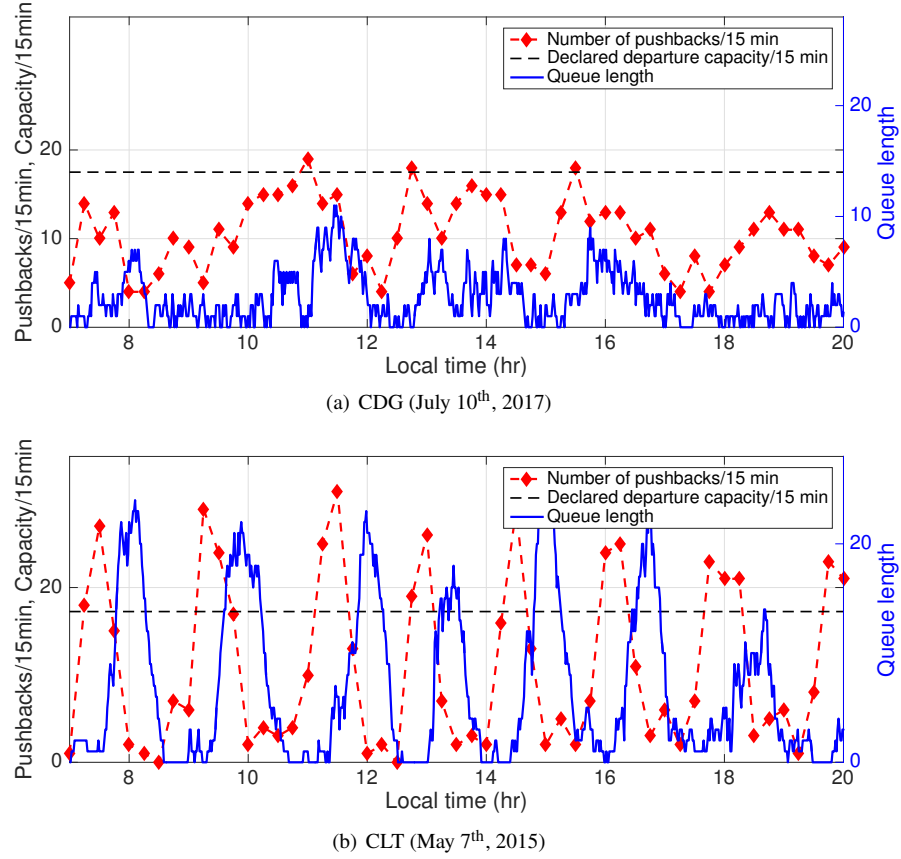
Fig. 2   Number of pushbacks (per 15 min), declared departure capacity and queue length for a typical good weather day.

nodes); minimum runway separation time between two consecutive flights f and g, denoted by s_{fg}.

2. Decision variables

For each flight $f \in \mathcal{F}$, the decision variables are defined as follows:

(a) CDG in West-flow runway configuration.

(b) CLT in North-flow runway configuration.

Fig. 3   Node-link network for the airport surface.

- p_f: Pushback time for departures (discretized), $p_f \in \{I_f, I_f + \Delta t, \cdots, I_f + N_p \cdot \Delta t\}$;

- w_f: Holding time (waiting time at runway threshold for departures and time spent in runway crossing queues for arrivals), $w_f \in \{0, \Delta t, 2 \cdot \Delta t, \cdots, N \cdot \Delta t\}$;

- v_f: Taxi speed, $v_f \in \{V^{\min}, V^{\min} + \Delta v, \cdots, V^{\max}\}$.

The pushback times (p_f) are the key decision variables in departure metering. However, the holding times at the runway (w_f) and taxi speeds (v_f) also need to be determined to ensure conflict-free solutions. The taxi speeds are determined for the pushback area, ramp and active movement area (AMA). The following auxiliary variables are introduced:

- t_f^u: Runway usage time (takeoff time for departures or runway crossing time for arrivals), based on taxi paths and speeds;

- t_f^c: Completion time for flight f: $t_f^c = t_f^u$ for departures, and the in-gate time for arrivals.

3. Constraints

The maximum holding delay and pushback delay are specified by Constraints (1) and (2), respectively. Constraint (3) defines the possible range of taxi speeds, when the aircraft is not stopped at a holding point.

$$0 \leq w_f \leq N \cdot \Delta t, \qquad \forall f \in \mathcal{F}, \tag{1}$$

$$I_f \leq p_f \leq I_f + N_p \cdot \Delta t, \qquad \forall f \in \mathcal{D}, \tag{2}$$

$$V_f^{\min} \leq v_f \leq V_f^{\max}, \qquad \forall f \in \mathcal{F}, \tag{3}$$

In order to introduce the runway separation constraints, we define the following sets to represent infeasible assignments of runway usage times. For any two distinct flights $f, g \in \mathcal{F}$, we introduce:

$$C_{fg}^R = \begin{cases} 1, & \text{if } (t_g^u - t_f^u < s_{fg} \text{ or } t_f^u - t_g^u < s_{gf}) \text{ and } r_f = r_g, \\ 0, & \text{otherwise;} \end{cases} \tag{4}$$

Then, the minimum runway separation requirement is guaranteed by Constraint (5):

$$\sum_{(f,g) \in \mathcal{F} \times \mathcal{F}, f \neq g,} C_{fg}^R = 0, \tag{5}$$

(a) Node separation   (b) Link overtaking   (c) Bi-link head-on
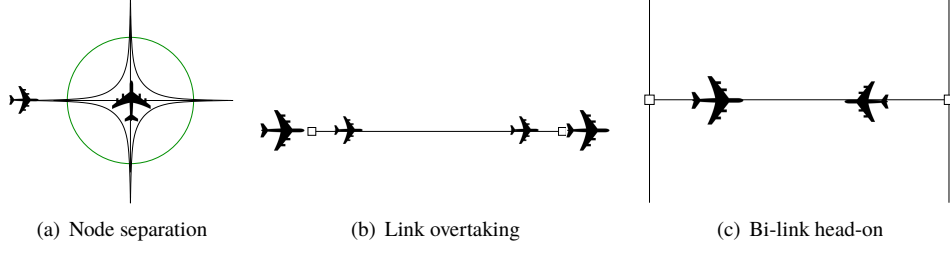
Fig. 4   **Taxi separation based on node-link network.**

For any two distinct flights $f, g \in \mathcal{F}$, we introduce:

$$
C_{fg}^H =
\begin{cases}
1, & \text{if } ((t_g^u - w_g < t_f^u - w_f \text{ and } t_g^u > t_f^u) \\
& \text{or } (t_f^u - w_f < t_g^u - w_g \text{ and } t_f^u > t_g^u)) \text{ and } h_f = h_g, \\
0, & \text{otherwise;}
\end{cases}
\tag{6}
$$

The first-come-first-served order is ensured at the holding point by Constraint (7),

$$
\sum_{(f,g) \in \mathcal{F} \times \mathcal{F}, f \neq g,} C_{fg}^H = 0,
\tag{7}
$$

Let $\mathcal{T} = 1, 2, ..., |\mathcal{T}|$ be the discretized time steps. We define a holding capacity indicator as follows, $O_{h,t} = \max\{\text{Card}\{f | h_f = h \text{ and } t_f^u - w_f \leq t \leq t_f^u\} - C, 0\}$. Then, Constraint (8) ensures that the number of aircraft waiting at the holding point does not exceed a specified limit,

$$
O_{h,t} = 0, \forall h \in \mathcal{H}, \forall t \in \mathcal{T}.
\tag{8}
$$

This limit depends on the airport layout for arrivals, and is an ATC-defined parameter (runway pressure) for departures.

We ensure a minimum taxi separation by considering three types of separation loss (Fig. 4): node separation, link overtaking separation, and bi-link head-on separation. Based on the node-link network, we can define:

- Node conflict: A node conflict is detected if the separation time between two successive aircraft using the node is less than the minimum separation time, which is calculated based on the safe separation distance, s, and the taxi speed. In order to specify a node conflict, we first define a *detection zone* as a disk of radius s centred at every node. Consider a scenario when an aircraft f enters the *detection zone* of node n before aircraft g (assuming both f, g have node n on their taxi route). We denote the entry time and exit time from the detection zone for aircraft f (g) as $t_{f,n}^{\text{In}}$ $(t_{g,n}^{\text{In}})$ and $t_{f,n}^{\text{Out}}$ $(t_{g,n}^{\text{Out}})$, respectively. A conflict is detected when $t_{g,n}^{\text{In}} < t_{f,n}^{\text{Out}}$, which means that aircraft g enters the detection zone before aircraft f exits. We define node conflict for aircraft f (leading) and g (following)

as follows:

$$N_{fg}^n = \begin{cases} 1, & \text{if } t_{g,n}^{\text{In}} < t_{f,n}^{\text{Out}}, \\ 0, & \text{otherwise}; \end{cases}$$

- Overtaking conflict on links: The entry and exit time of each flight passing through a link are compared to check if the entry order of aircraft differs from the exit order. An overtaking conflict occurs when the entry and exit orders are different. For two consecutive flights f, g that pass through a link $l = (m, n)$ in the same direction, the link conflict is defined as:

$$L_{fg}^l = \begin{cases} 1, & \text{if } (t_f^m < t_f^n \text{ and } t_g^m < t_g^n \text{ and } t_g^n < t_f^n) \text{ or } (t_f^n < t_f^m \text{ and } t_g^n < t_g^m \text{ and } t_g^m < t_f^m), \\ 0, & \text{otherwise}; \end{cases}$$

Here, t_f^m is the passage time of flight f at node m.

- Head-on conflict on links: A head-on conflict occurs when the exit time of an aircraft using a link is earlier than the entry time of another aircraft using the same link but heading in the opposite direction. For two consecutive flights f, g that pass through a link $l = (m, n)$ in the opposite direction, the head-on conflict is defined as:

$$L_{fg}^b = \begin{cases} 1, & \text{if } (t_f^m < t_f^n \text{ and } t_g^n < t_g^m \text{ and } t_g^n < t_f^n) \text{ or } (t_f^n < t_f^m \text{ and } t_g^m < t_g^n \text{ and } t_g^m < t_f^m), \\ 0, & \text{otherwise}; \end{cases}$$

- $C_t = \sum\limits_{\substack{f,g \in \mathcal{F}, \\ f \neq g}} (\sum\limits_{n \in \gamma_f \cap \gamma_g} N_{fg}^n + \sum\limits_{l \in \gamma_f \cap \gamma_g} (L_{fg}^l + L_{fg}^b)) = 0$ ensures that there are no ground conflicts.

4. Objective function

The objective is to minimize

$$\alpha \Phi_p + \beta \Phi_d + \gamma \Phi_a,$$

where α, β and γ are weighting coefficients, and where Φ_p is the average pushback delay, Φ_d is the average taxi-out time, and Φ_a is the average taxi-in time. The conflict-avoidance constraints are handled by performing the following relaxation to the objective function,

$$\Phi_c + \theta(\alpha \Phi_p + \beta \Phi_d + \gamma \Phi_a)$$

where $\Phi_c = C_t + \sum\limits_{\substack{f,g \in \mathcal{F} \\ f \neq g}} (\sum\limits_{h \in h_f \cap h_g} C_{fg}^h + \sum\limits_{R \in R_f \cap R_g} C_{fg}^R) + \sum\limits_{h \in \mathcal{H}} \sum\limits_{i \in \mathcal{T}} O_{h,i}$, and θ is a weighting coefficient, which is set to a small value to ensure that the conflicts are prioritized in the minimization. A conflict occurs when aircraft violates the minimum separation requirement. Once a conflict-free solution is reached, the system continues to minimize other

criteria.

B. Solution approach to trajectory-based node-link model

The solution to the optimization problem is obtained using an adapted simulated annealing (SA) algorithm [25]. At each iteration in the algorithm, a neighboring solution to the current solution is generated, and the neighboring solution is accepted with a probability that depends on the difference in objective function between the two solutions and a temperature parameter. The temperature parameter is progressively reduced with each iteration, thereby modulating the exploration of the solution space.

C. Model parameters

The node-link model for CDG (Fig. 3(a)) consists of 1,185 nodes and 1,441 links with 517 gates. The model for CLT (Fig. 3(b)) consists of 581 nodes and 506 links, with 102 gates. Aircraft are assumed to taxi with a constant speed within each link. However, aircraft's speed can vary between links within the minimum and maximum value. There is no restriction of the speed between adjacent links. Additionally, aircraft can stop only at the gates and runway holding points. The range of taxi speeds are obtained from operational data. The maximum taxi speeds at CDG are assumed to be 0.3, 7.0, and 10.0 m/s for the pushback area, ramp area, and AMA, respectively. The equivalent values for CLT are assumed to be 0.15, 7.0, and 9.0 m/s. The minimum speed is assumed to be half the maximum speed in the ramp area and AMA, and 80% of the maximum taxi speed in the gate area. The minimum taxi separation is considered to be 60 m in the AMA and 30 m in the ramp area at CDG [14, 15], and 80 m on taxiways and 30 m in the ramp area at CLT based on flight track visualizations. Given an origin (gate or runway exit) and a destination (runway entry or gate) pair, a taxi route is defined as a set of nodes and links connecting the origin to the destination. Taxi routes are obtained from historical data for the two airports. The runway separation time was obtained as the mean of the empirical distribution obtained from operational data and consistent with the separation time distribution used for the macroscopic model.

The other user-defined parameters in the optimization are as follows: $\Delta t = 5$ s and $\Delta v = 0.01 V_f^{\max}$. Since CLT is more congested than CDG, the maximum gate-holding time is considered to be 25 min at CLT and 10 min at CDG. Moreover, due to the different layouts of the arrival holding areas at the two airports, we assume that a maximum of 2 arrivals can wait at the holding point at CDG, and 5 arrivals at CLT. The maximum holding time for arrivals is 10 min at CLT and 5 min at CDG. The maximum holding time for departures is 20 min at CLT and 15 min at CDG, and a maximum of 5 departures can wait at the runway threshold for both airports. The weighting coefficients for the objective function are set to $\alpha = 2$, $\beta = 1$ and $\gamma = 1$ at CLT, and $\alpha = 1$, $\beta = 1$ and $\gamma = 0.01$ at CDG. These coefficients are chosen such that the average wheels-off delay due to departure metering is minimized.

D. Expected benefits of trajectory-based optimization

The baseline taxi-times are computed with only the taxi speeds and holding times at the runway threshold as the decision variables in the optimization process. For the metering case, the pushback time is included as an additional decision variable. Fig. 5(a) shows the optimized taxi-times averaged over 15-min intervals for a typical day at CLT. We can see the taxi-out and taxi-in time reductions in the optimized case, particularly during time intervals that have a high baseline value. This reduction in taxi-in time arises primarily from the better sequencing of runway crossings. Note that the reduction in taxi-out time does not adversely impact the taxi-in time. The reduction in taxi-out time corresponds to reduced queue lengths on the airport surface (Fig. 5(b)).

(a) Taxi times averaged over 15 min windows

(b) Total departure runway queue length
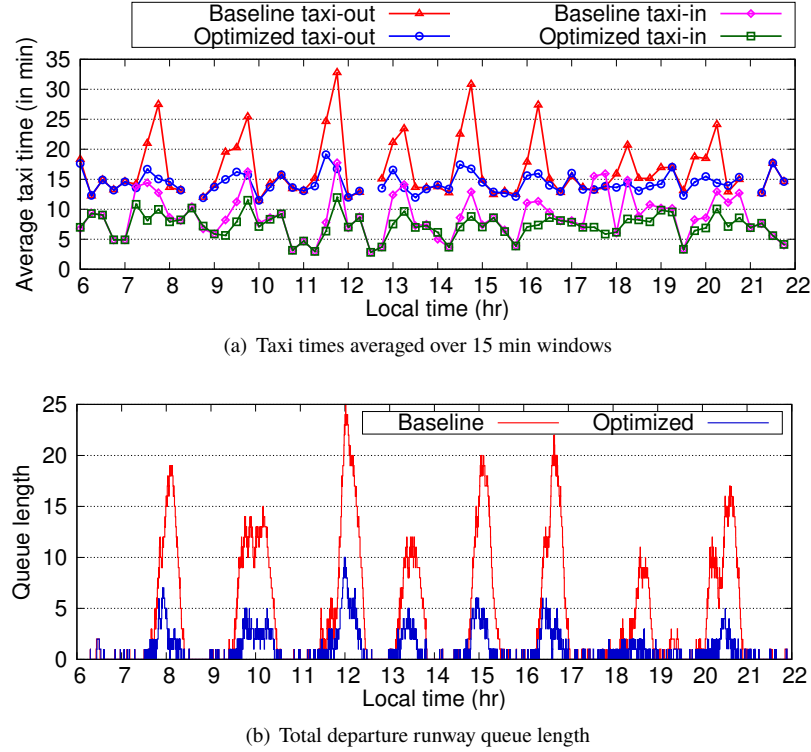
Fig. 5 Comparison of queue length and taxi-time with trajectory-based departure metering for a typical day at CLT (May 7th, 2015).

Aggregate statistics over a three day period (6 AM to 10 PM local) at the two airports are presented in Table 1. As one would expect, the taxi-out time reduction is higher at CLT (3.5 min) compared to CDG (1 min). Moreover, the average hold time does not exceed the average taxi-out time reduction, resulting in no additional wheels-off delay from metering. In fact, the wheels-off delay is *negative* at CLT because of an increase in throughput of about 3% from better sequencing of arrival runway crossings and takeoffs.

Table 1   Trajectory-based departure metering: Aggregate statistics.

Average values	CLT	CDG
Baseline taxi-out time (min)	18.4	14.2
Taxi-out time reduction with metering (min)	3.5	1.1
Baseline taxi-in time (min)	9.6	10.1
Taxi-in time reduction with metering (min)	1.7	0.0
Gate-hold time (min)	3.0	1.1
Wheels-off delay (min)	-0.5	0.0
Percentage of flights held at the gate	61%	50%

IV. Queuing-based approaches

In this section, we consider a different class of departure metering algorithms that are based on queuing network models of the airport surface. The queuing models differ from the microscopic trajectory-based approach presented earlier in that they output macroscopic quantities such as queue lengths and taxi-out times. These macroscopic models are easier to adapt to different airports, and lend themselves to efficient model-based control strategies for departure metering. In contrast to the trajectory-based approach that controls both arrival and departure trajectories, the queuing-based approaches regulate only the times (or rate) at which aircraft depart from their gates. However, the interactions between arrivals and departures are modeled and can be simulated.

A. Queuing network models

The main goal of a queuing network model of the airport surface is to determine queue lengths and taxi-out times as a function of the pushback times and other input parameters.

1. Fluid-flow model for queues

The fluid model is a continuum approximation to the discrete queuing problem. Let $\lambda(t)$ be the mean in-flow rate into the queue and $\mu(t)$ be the mean service rate of the server. Then, the dynamics of the queue length ($x(t)$) is given by the following equation [19]:

$$\dot{x}(t) = -\mu(t)\frac{C(t)x(t)}{1 + C(t)x(t)} + \lambda(t),\qquad(9)$$

where C is a positive parameter that depends on the coefficient of variation of the service time distribution of the server [19]. The negative term in the above equation is the mean out-flow rate from the queue. Using the principle of flow-conservation, the model can be extended to a network of queues, using the fact that the output of one queue becomes the input to the next, if they are connected.

2. Queuing network model of CDG

The runways are the primary bottleneck at CDG, leading to the formation of departure runway queues. The taxi-out process is represented using a single queue, one for each departure runway as shown in Fig. 6(a). After pushback, an aircraft enters the departure runway queue after spending an unimpeded gate-to-runway time. The dynamics for the evolution of the departure runway queues are given by

$$\dot{x}_{r_i} = -\mu_{r_i}(t)\frac{C_{r_i}(t)x_{r_i}(t)}{C_{r_i}(t)x_{r_i}(t) + 1} + u_{d_i}(t - \tau_{gr_i}), \ i = 1, 2 \tag{10}$$

where x_{r_i} represents the queue length of the ith departure runway, and τ_{gr_i} is the average unimpeded travel time from the gate to the ith departure runway, u_{d_i} represents the pushback rate to the ith departure runway. The pushback rate is computed as the number of aircraft pushing back from the gate in a given time interval (5 min in this paper). The time delay in the dynamics accounts for the travel time from the gate to the departure runway.

The queue length can be predicted by integrating the dynamics forward in time with appropriate server parameters and pushback rate. The wait times of aircraft entering the queue are determined using the predictions of queue length and time-varying mean service rates [20]. The taxi-out time is then determined as the sum of the unimpeded gate-to-runway time plus the waiting time in the queue. The unimpeded times are computed as the 10th percentile of the empirical taxi-time distribution obtained from data.

3. Queuing network model of CLT

CLT experiences significant congestion in the ramp area, in addition to queuing at the departure runways. Therefore, the CLT model includes a ramp queue and two departure runway queues (Fig. 6(b)). After pushback, departures enter the ramp queue, followed by one of the two runway queues based on the runway assignment. We model the ramp queue as a multi-class queue, the class of customers representing the runway assignment of the aircraft in the queue. The service rate for a particular class is assumed to be proportional to the number of customers of that class in the queue. The queuing dynamics is then given by

$$\dot{x}_{s_i} = -\mu_s(t)\frac{C_s(t)x_{s_i}(t)}{C_s(t)x_s(t) + 1} + u_{d_i}(t - \tau_{gs}); \ x_s = \sum_{i=1}^{2} x_{s_i} \tag{11}$$

$$\dot{x}_{r_i} = -\mu_{r_i}(t)\frac{C_{r_i}(t)x_{r_i}(t)}{C_{r_i}(t)x_{r_i}(t) + 1} + \frac{\mu_s(t - \tau_{si})C_s(t - \tau_{si})x_{s_i}(t - \tau_{si})}{C_s(t - \tau_{si})x_s(t - \tau_{si}) + 1}, \tag{12}$$

where x_{s_i} represents the number of aircraft in the ramp queue that are bound for the ith departure runway, τ_{gs} is the average unimpeded travel time from the gate to the spot, and τ_{si} represents the average unimpeded travel time from the spot to the ith runway ('spot' refers to the exit of the ramp area into the active movement area).

Arrivals and departures at CLT interact in the ramp area. Therefore, the taxi-in process at CLT is represented as

13

follows: flights landing on the leftmost runway (36L) pass through a runway crossing queue and a taxi-in ramp queue, whereas flights landing on one of the other runways just pass through the taxi-in ramp queue (see Fig. 6(b)). Additional details on the queue model for CLT can be found in our earlier work [20].

4. Service time distributions

Empirical service time distributions are obtained as the difference between successive exit times from the queue when there is a non-zero queue length. The service time distribution of a departure runway server is conditioned on the number of landings and the weather (IMC/VMC) for each 5-min window. The mean service rate of the departure runway server was found to decrease with increase in the number of landings because runway is shared between takeoffs and landings for mixed operations. On the other hand, congestion in the ramp area is primarily because of flights sharing common taxi-paths while heading in different directions. The arrival traffic flow from the spot to the gates impedes the departure movement in the ramp area. Therefore, the service time distribution of the taxi-out ramp server is modelled as a function of the length of the taxi-in ramp queue, and vice versa [20]. The impact of fleet mix was not explicitly considered in the queue model because only a small percentage of aircraft at CLT (2%) belong to the 'heavy' category of aircraft weight class. For CDG, although the percentage of aircraft that belong to the 'heavy' category is higher, we did not find a significant improvement in the predictive performance by conditioning the service time distribution with the aircraft fleet mix. The primary reason being that the 'heavy' followed by 'large' sequence, which has a higher runway separation time requirement, occurs only 12% of the time at CDG.
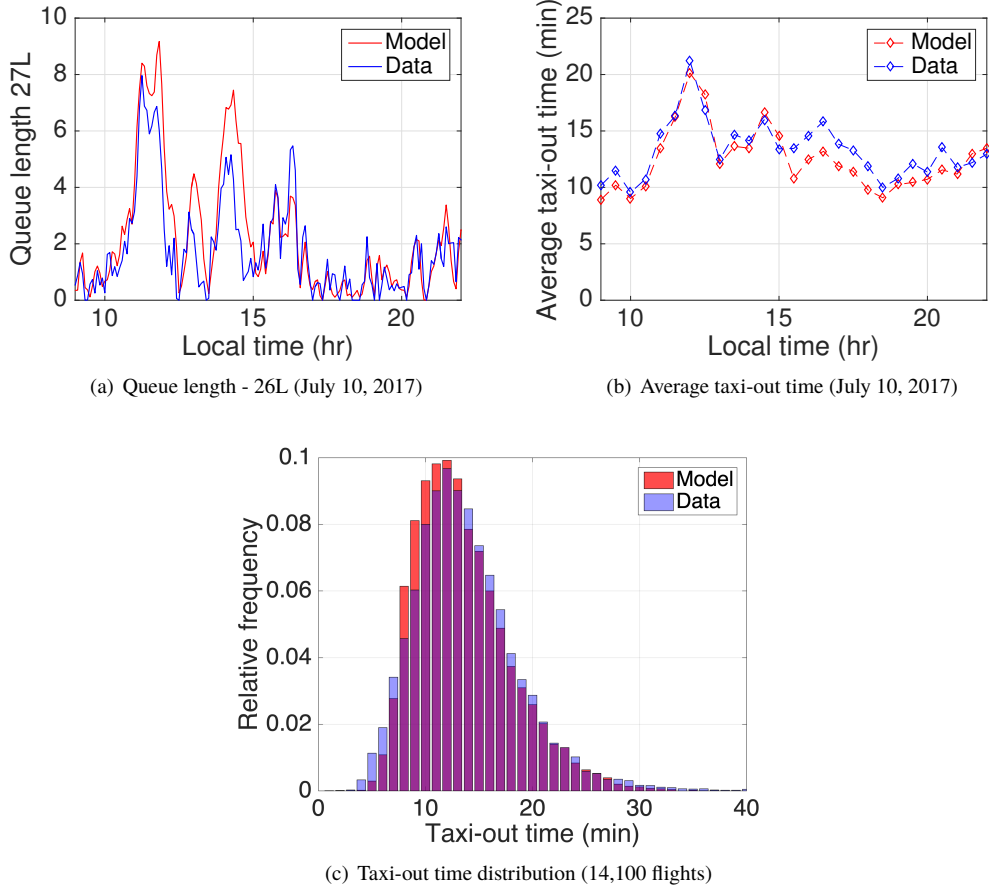
5. Predictive performance of queuing models

Fig. 7(a) shows a comparison of the predicted and observed departure runway queue lengths at CDG for a typical day. The data corresponds to a time-based definition of queue length, in which an aircraft is said to be in the runway queue if it has spent unimpeded gate-to-runway time after pushback but is yet to take-off. The taxi-out times for this

(a) CDG in West-flow runway configuration.   (b) CLT in North-flow runway configuration [20].
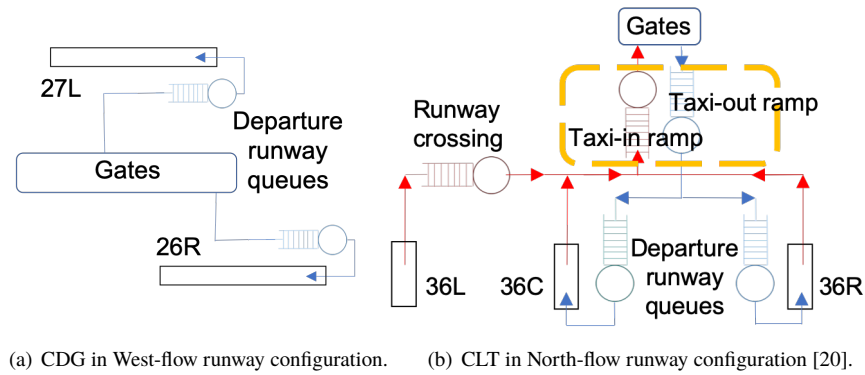
Fig. 6   Queuing representation for the surface traffic

particular day, averaged over 15-min windows, are shown in Figure 7(b). These figures show a good match between the predictions and observed values. A similar match is also observed for CLT [20].

(a) Queue length - 26L (July 10, 2017)

(b) Average taxi-out time (July 10, 2017)

(c) Taxi-out time distribution (14,100 flights)

Fig. 7   Comparison between model predictions and data for CDG.

Table 2   Error statistics using analytical queue models.

Airport	Number of departures	Taxi-out time (min)			% of flights |error| < 5 min
		Mean	ME	MAE	
CDG	14,100	13.3	-0.3	3.0	82.4
CLT	7,464	20.1	-1.4	4.4	69.0

Table 2 shows the aggregate error statistics of taxi-out time prediction for individual flights, computed for an independent test set of 14,100 departures for CDG and 7,464 departures at CLT. Here, the errors are computed as the predicted taxi-out time minus the actual value. Flights with taxi-out times greater than 50 min were not included while computing the statistics (50 min represents the 99th percentile of the taxi-out time distribution at CLT). The mean errors (ME) and mean absolute errors (MAE) are found to be small relative to the mean taxi-out times. The errors for CLT are slightly higher than CDG because of higher uncertainty in the ramp operations at CLT. Although the MAE for CLT is

15

more than CDG, one needs to note that the relative error (MAE/(mean taxi-out time)) is similar at the two airports. A good overlap can be seen between the predicted and actual taxi-out time distributions (Fig. 7(c)). The mean error is slightly negative for both airports. From the point of view of departure metering, positive errors are not desirable since they correspond to an over-prediction of taxi-out times, leading to overly-aggressive holds and unnecessary wheels-off delays.

B. Queue-based departure metering approaches

A simple differential equation representation of the queuing dynamics allows us to develop efficient strategies for controlling the pushback time at the gate to reduce queue lengths (and taxi-out times). Three departure metering approaches based on the queuing model are considered: a rule-based heuristic (representative of NASA's ATD-2 logic), an optimal control method, and a robust control based technique that explicitly accounts for model uncertainties.

1. Rule-based heuristic

The rule-based heuristic is representative of NASA's ATD-2 logic for departure metering. The heuristic computes a gate-hold time for each flight based on its predicted taxi-out time as follows [2]:

$$TOBT = \max(EOBT, TTOT - UTT - Y),\tag{13}$$

where $TOBT$ is the Target-Off-Block-Time or the new gate release time determined by the departure metering algorithm, $TTOT$ is the Target Take-Off-Time, UTT is the unimpeded time to take-off that depends on the gate-runway pair, Y is the excess queue time buffer and $EOBT$ is the Earliest Off-Block Time. $EOBT$ is the expected push ready time published by the airlines. We use the FAA's Surface CDM* (S-CDM) nomenclature, which differs slightly from the Airport CDM (A-CDM) notation, for the data elements [7]. For purposes of simulation in this paper, the actual pushback time from historical data is assumed to be the EOBT. In other work, we have considered the accuracy and uncertainty associated with the EOBT as reported by the airlines [26]. The target takeoff time is computed by adding the predicted taxi-out time to the flight's EOBT. The queuing model presented earlier is used to obtain the predicted taxi-out time for each flight. In other words, the hold time assigned to each flight is the predicted wait time in queue for that flight minus the excess queue time buffer:

$$\text{gate-hold-time} = \max(\text{predicted wait-time} - Y, 0).\tag{14}$$

The underlying idea is to transfer the predicted wait time in the queues to a gate-hold time, thereby saving fuel. To improve operational predictability, the hold decisions are made T_p minutes prior to a flight's EOBT, where T_p is the planning horizon. A larger planning horizon leads to higher predictability of the gate hold-decisions, but results in lower

---

*CDM: Collaborative Decision Making
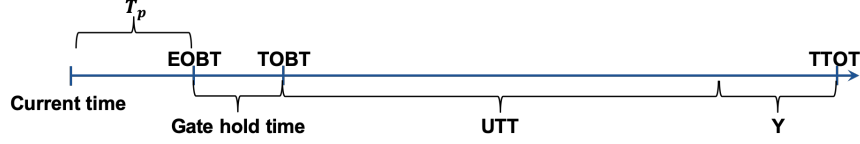
Fig. 8   A timeline diagram representing the rule-based heuristic as simulated.

metering benefits because of the higher uncertainty in the taxi-out time prediction. We have considered a planning horizon of 20 min, which is within the range of consideration by NASA under the ATD-2 concept. A timeline diagram of the rule-based heuristic is shown in Fig. 8.

The excess queue time buffer (Y) helps accommodate errors in taxi-out time prediction. It is important to choose an appropriate value for this parameter: If too high, it will lead to decreased benefits; and if too low, it could lead to reduced runway utilization. The optimal buffer is chosen such that it yields the maximum reduction in taxi-out time while ensuring that the average change in wheels-off time is less than 0.1 min. The optimal excess queue time buffer for a 20 min planning horizon was determined to be 6 min for CDG, and 7 min for CLT, based on stochastic simulations (Section. V.A) of operations over a 15-day period. The impact of planning horizon and the choice of excess queue time buffer for CLT has been investigated in our earlier paper [26]. A larger buffer is to be expected for CLT, since as seen in Table 2, the queuing model errors are larger for CLT than CDG.

2. Optimal control approach

The optimal control approach determines hold times by explicitly optimizing the queue lengths on the airport surface instead of using a rule-based heuristic. We have presented the optimal control approach and applied it for CLT in our earlier work [27]. We briefly discuss the approach again here for the sake of clarity.

In the optimal control approach, the pushback rate is determined as a solution to an optimal control problem. The control objective tries to penalize a weighted sum of the square of the queue lengths (to reduce taxi-out times) and number of holds (to avoid having large holds and to maintain runway throughput). The optimal control problem

formulation is then as follows:

$$\min_{\mathbf{u_d}(t)} \int_0^T \left(\mathbf{x}^\mathrm{T} Q \mathbf{x} + \mathbf{h}^\mathrm{T} R \mathbf{h}\right) dt \tag{15}$$

Subject to: (16)

$$\dot{\mathbf{x}} = \mathbf{f}(\mathbf{x}(t), \mathbf{x}(t - \tau_1), \dots \mathbf{x}(t - \tau_m), \mathbf{u}_d(t - \tau_{m+1}), \dots \mathbf{u}_d(t - \tau_w), t) \tag{17}$$

$$\dot{\mathbf{h}} = \mathbf{d}(t) - \mathbf{u_d}(t) \tag{18}$$

$$0 \le x_i, \ i = 1, 2, 3, \dots m; \ \ 0 \le h_i, \ \ 0 \le u_{di} \le u_{\max}; \ i = 1, 2, 3, \dots w \tag{19}$$

$$u_{di}(t) = g_i(t), \ t \in [-\tau_{di}, 0); \ i = 1, 2, 3, \dots w \tag{20}$$

$$x_i(t) = \phi_i(t), \ \ t \in [-\tau_{ki}, 0], \ \mathbf{h}(0) = \mathbf{h}_0; \ i = 1, 2, 3, \dots w \tag{21}$$

Here, T is the time horizon over which the cost needs to be minimized, $\mathbf{x}(t) \in \mathbb{R}^m$ is a vector of taxi-out queue lengths (including ramp queues if present), $\mathbf{h}(t) \in \mathbb{R}^w$ is the number of aircraft held at their gates due to departure metering and $\mathbf{d}(t) \in \mathbb{R}^w$ is the departure demand rate, with its elements representing the demand rate to each runway. The departure demand corresponds to the push-ready time for departures (obtained from the EOBTs), averaged over 5-min windows. Additionally, $\mathbf{u_d}(t) \in \mathbb{R}^w$ is the pushback rate to each runway that needs to be determined, and Q and R are constant weighting matrices of appropriate dimensions. Equations (17) and (18) specify the dynamics for the length of the queues and number of holds. The inequalities in (19) impose nonnegativity constraints on the number of holds, queue lengths, and pushback rate. The delay differential equations also require an initial history, specified by Equations (20)-(21).

The service time distributions for the departure runway queues depend on the landing rates and meteorological conditions, which are assumed to be known. For CLT, the taxi-in ramp queue length is pre-computed using the queuing model with the EOBTs and arrival times, and is used to determine the service rate for the taxi-out ramp queue.

A receding horizon framework is adopted to solve the optimal control problem so that the pushback decisions are based on the current state of the airport surface. The day is divided into 5-min intervals. At the beginning of each interval, t, the optimal control problem is solved for $[t + T_p, t + T_p + T]$ where T_p is the planning horizon, and T is the time-period over which the cost is minimized. At that time, the pushback rate is decided only for the next 5 min, namely, $[t + T_p, t + T_p + 5]$ min. The initial conditions for T_p min into the future are obtained using the queuing model with the current state of the airport as the input. The number of aircraft that can be released during each 5-min window (n) is determined from the pushback rate. The first n aircraft in the 5-min window are released as per the optimal control decision, and remaining aircraft are pushed to the beginning of the next time window, awaiting decision for release. In contrast to the rule-based heuristic which assigns and freezes the hold times for flights that have an EOBT T_p min ahead, the optimal control approach only specifies the flights that need to be released in $[t + T_p, t + T_p + 5]$ time window, and

postpones the remaining flights to the next time window. In other words, the gate-hold time for a flight is determined T_p min prior its EOBT in the rule-based heuristic, whereas, the gate-release time for a flight is determined T_p min prior to its planned gate-release time in the optimal control approach. Consequently, aircraft can be postponed multiple times to the next time window in the optimal control approach. However, a final pushback time is frozen T_p minutes ahead.

The optimal control problem is solved numerically by discretizing the state and control variables due to the challenges posed by time delays and nonlinear dynamics. The equations are discretized using a first-order Euler method, and the resulting non-linear programming problem (NLP) is solved using a standard solver in MATLAB. Appropriate weight functions to avoid loss in runway utilization were found to be $R = 0.4I$ and $Q = I$ for a 20 min planning horizon (T_p). The time-period over which the cost is minimized (T) is considered to be 30 min for CLT and 60 min for CDG. The larger time-period at CDG is due to its wider departure banks.

3. Robust control

The optimal control approach relied on the predictions of the queuing model to determine the pushback rate. However, these predictions can be inaccurate. The robust control strategy regulates the pushback rate to achieve a target departure runway queue length while explicitly accounting for model uncertainties. Sliding mode control, a standard technique in robust nonlinear control, is adopted to account for model uncertainties [28]. To handle the challenges posed by time-delays, we first ignore their effect, and then use predictor-based feedback to account for them [29].

For illustrative purposes, we only present the methodology for CDG. The model for the taxi-out queue dynamics (Eq. (10)) without the time-delay is given by:

$$\dot{x}_{r_i} = -\mu_{r_i}(t)\frac{C_{r_i}(t)x_{r_i}(t)}{C_{r_i}(t)x_{r_i}(t) + 1} + u_{d_i}(t) = \bar{\alpha}_i(x_{r_i}, t) + u_{d_i}(t), \; i = 1, 2 \tag{22}$$

where $\bar{\alpha}_i(x_{r_i}, t) = -\mu_{r_i}(t)\frac{C_{r_i}(t)x_{r_i}(t)}{C_{r_i}(t)x_{r_i}(t)+1}$. The objective is to determine the pushback rate ($u_{d_i}(t)$) in order to maintain the queue length of departure runway i (denoted x_{r_i}) at a desired value, $x_{r_i,d}$. We assume that the actual dynamics deviates from the model, but has the following structure

$$\dot{x}_{r_i,a} = \alpha_i(x_{r_i,a}, t) + u_{d_i}(t), \; i = 1, 2, \tag{23}$$

where $x_{r_i,a}$ represents the actual queue length and $\alpha_i(.)$ is an unknown function that is bounded as follows:

$$|\alpha_i(x_{r_i,a}, t) - \bar{\alpha}_i(x_{r_i,a}, t)| \le F_i(x_{r_i,a}, t), \; i = 1, 2 \tag{24}$$

Motivated by the fact that the errors arise primarily due to uncertainties in the individual service times, we consider the following form for $F_i(x_{r_i,a}, t) = a_i\frac{C_{r_i}(t)x_{r_i,a}(t)}{C_{r_i}(t)x_{r_i,a}(t)+1}$. Here, a_is are design parameters that need to be chosen depending

19

on the level of uncertainty.

The asymptotic tracking of the queue length can be achieved using a fairly standard technique [28]. The resulting feedback law is given by:

$$u_{d_i}(t) = \max\left(-\bar{\alpha}_i(x_{r_i,a}(t), t) - k_i \operatorname{sat}(x_{r_i,a}(t) - x_{r_i,d}), 0\right). \tag{25}$$

Here, the gain parameter (k_i) needs to be chosen to satisfy $k_i > F_i(x_{r_i,a}, t)$ and sat(.) represents the saturation function, defined as

$$\operatorname{sat}(x) = x, \text{ if } |x| < 1; \text{ and } \operatorname{sgn}(x), \text{ otherwise.} \tag{26}$$

In the control law (25), instead of the states at the current time, t, the predicted states at time, $t_{pred} = (t + T_p + \tau_{gr_i})$ are used to handle delay in the queuing dynamics (τ_{gr_i}) and to account for the planning horizon (T_p). The predicted queue length ($x_{r_i,p}$) is obtained by integrating the queuing dynamics (10) forward in time using the current queue length as the initial condition. The pushback rate at time t is given by:

$$u_{d_i}(t) = \max\left(-\bar{\alpha}_i(x_{r_i,p}(t_{pred}), t_{pred}) - k_i \operatorname{sat}(x_{r_i,p}(t_{pred}) - x_{r_i,d}), 0\right). \tag{27}$$

The pushback rate decisions are converted into flight-specific holds as described earlier in the optimal control framework. A pushback rate control law can be derived for CLT using the same principles.

The target queue length is set to 3.25 at CDG and 3.75 at CLT based on simulations, to obtain maximum reduction in taxi-out time while ensuring no significant loss in runway throughput. The gain parameters (k_i) are appropriately picked.

V. Comparison of departure metering algorithms

A. Simulation environment

The departure metering approaches are evaluated using simulations of airport surface operations. The simulators are based on discrete versions of the queuing network models (as described in Section IV), with the service time for each server being sampled from an empirical distribution. The empirical service time distributions are a function of the airport weather, and traffic, as discussed earlier in Section IV.A.4. Additionally, the departure runway service time distributions for CDG depends on the leading and trailing aircraft weight category since CDG handles a significant number of heavy aircraft.

The service times are randomly sampled from the empirical distributions and the simulations repeated multiple times to obtain consistent statistics (a Monte Carlo simulation with 10 runs). Table 3 validates the simulations by comparing the taxi-out time predictions from the simulator in the baseline case (without any metering) to actual data

over multiple days. The results indicate that the simulations are quite accurate, and that the errors are small relative to the mean taxi-out times.

Table 3   Error statistics for stochastic simulations of baseline.

Airport	Number of departures	Taxi-out time (min)			% of flights |error| < 5 min
		Mean	ME	MAE	
CDG	14,202	13.3	-0.3	3.0	84.0
CLT	6,474	20.1	1.1	4.6	64.2

B. Comparison of benefits using stochastic simulations

The stochastic simulations are used to evaluate the benefits of departure metering for three days of operations (6AM-10PM local time). This case corresponds to 1,934 departures at CDG set (baseline mean taxi-out time of 12.8 min) and 1,903 departures at CLT (baseline mean taxi-out time of 21.0 min). For the queue-based approaches, the departure metering decisions are made with a planning horizon (T_p) of 20 min, using the information about the current state of the airport. For the trajectory-based approach, the modified pushback time is pre-computed for the entire day based on the expected off-block time (considered to be the actual off-block time from historical data).

Fig. 11 shows the taxi-out time averaged over 15-min windows with different departure metering approaches, and they are compared with the baseline case for a typical day at CLT. In general, we note that the spikes in taxi-out time seen in the baseline case are reduced with departure metering. Table 4 shows some key statistics obtained from the simulation, comparing the performance of the four approaches for CLT over the three days. The taxi-out time reduction reported in the table is the taxi-out time (pushback to wheels-off) in the baseline simulation minus that in the metering simulation. The wheels-off delay is computed as the wheels-off time with metering minus that in the baseline simulation. The benefits in terms of taxi-out time reduction range between 6-14% of the mean taxi-out time. Table 5 shows the departure metering statistics for CDG from the three days of simulation.

C. Discussion

Based on the results of the simulations in Sec. V.B, we make the following observations:

- As was expected from Fig. 2, the benefits of departure metering at CLT are expected to be significantly larger than those at CDG. This is in large part because the demand at CDG only occasionally exceeds its capacity, due to slot-constraints.
- The simulated taxi-out time savings at CLT are the highest for the robust control approach, followed by the rule-based heuristic, trajectory-based, and optimal control approaches, in that order. While the order of the last two of these is switched for CDG, we note that this is primarily because the baseline taxi-out times of the node-link model used by the trajectory-based approach deviate significantly from the observed values at CDG during the

21

most congested bank of operations (10AM-12PM local time).

- The longest hold times are prescribed by the trajectory-based approach, and the resulting taxi-out time savings are less than the hold times. In other words, the unnecessary wheels-off delays are the largest for the trajectory-based approach. The main reason for this is that the trajectory-based approach assumes the ability to control pushback times as well as the taxi routes and speeds along every link; in reality, these are uncertain quantities. As a result, the stochastic simulations reveal the "brittleness" of the deterministic solution in the current operating environment. However, it is reasonable to expect that as trajectory-based operations are adopted on the airport surface, the uncertainty associated with taxi times will decrease, and the resulting taxi-out time reductions will be closer to the solution of the trajectory-based approach.

- Fewer flights are held, but for a longer duration, with the robust controller compared to the other approaches. The gate hold-time distributions of the flights held at the gate for the rule-based heuristic and the robust control approach are shown in Fig. 9 and Fig. 10, respectively. Overall, the hold time of the flights held at the gate is relatively small for all the approaches, a desirable performance metric so that departures on hold don't occupy the gate long enough to create a conflict with the next arriving aircraft using the same gate.

- The taxi-out time reduction with departure metering leads to significant fuel burn savings. For example, the average fuel flow rate per flight during the taxi phase at CLT is 0.17 kg/s. Therefore, one can potentially save 29.5 kg of fuel per flight on average at CLT using the robust control approach for departure metering.


(a) CDG

(b) CLT
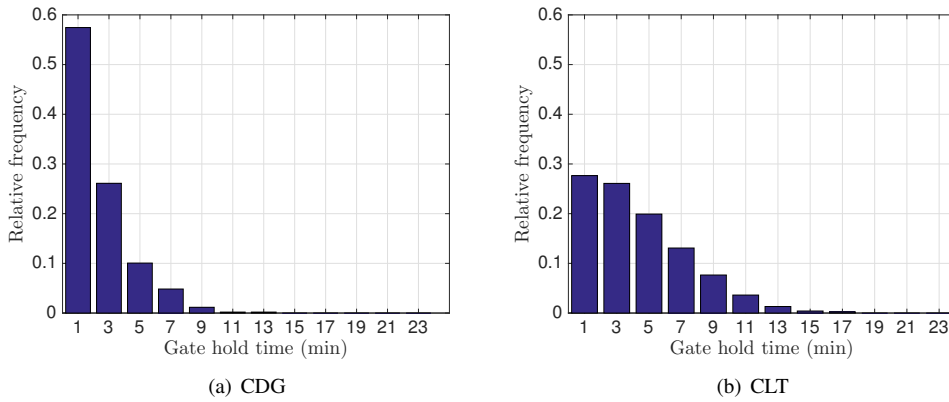
Fig. 9 Distribution of the gate hold-time of the flights held at the gate using rule-based heuristic.

In general, the algorithms that account for uncertainty perform better than those that do not, in the simulations. The robust control approach explicitly accounts for model uncertainties while determining the pushback rates. In the rule-based heuristic, the buffer parameter is appropriately picked to account for model uncertainties. The optimal control approach and the trajectory-based optimization approach optimize the pushback decisions based on deterministic models, and underperform in stochastic environments.

(a) CDG

(b) CLT
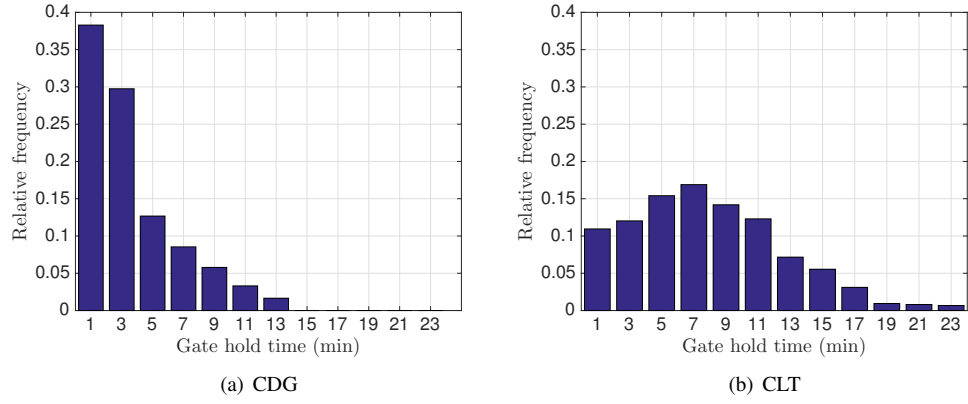
Fig. 10 Distribution of the gate hold-time of the flights held at the gate using robust control approach.
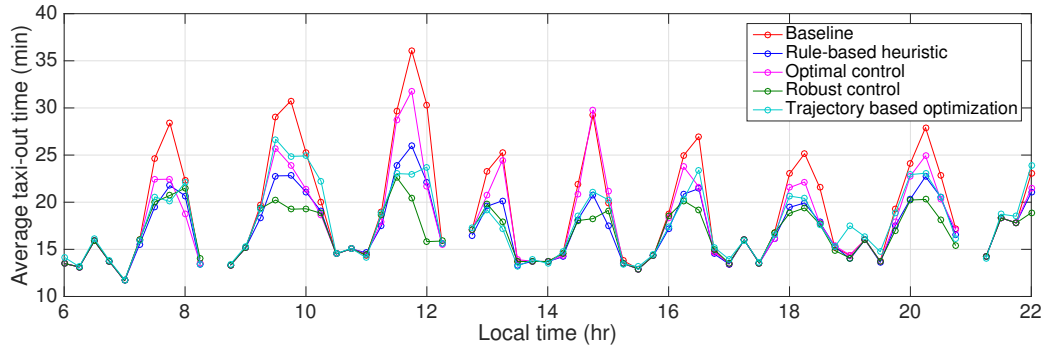
Fig. 11 Average taxi-out (per 15-min) with departure metering at CLT for a typical day (May 7, 2015).

Table 4   Comparison of simulations of departure metering approaches for CLT.

Mean statistics	Trajectory based	Rule-based heuristic	Optimal control	Robust control
Taxi-out reduction (min)	2.22	2.6	1.31	2.89
Hold time (min)	3.04	2.71	1.51	2.97
Wheels-off delay (min)	0.81	0.10	0.21	0.08
Fraction of flights held	0.61	0.63	0.34	0.35
Hold time of flights held (min)	4.96	4.33	4.50	8.40

Table 5   Comparison of simulations of departure metering approaches for CDG.

Mean statistics	Trajectory based	Rule-based heuristic	Optimal control	Robust control
Taxi-out reduction (min)	0.16	0.52	0.39	0.53
Hold time (min)	1.12	0.61	0.52	0.65
Wheels-off delay (min)	0.97	0.09	0.12	0.12
Fraction of flights held	0.50	0.26	0.17	0.17
Hold time of flights held (min)	2.2	2.36	3.09	3.96

23

The computational times for CLT are higher compared to CDG because of a more complex queuing network and higher traffic. In general, for every 5-min window receding horizon, the computational times are the highest for trajectory-based optimization (mean: 23 s; max 78 s at CLT), followed by the optimal control approach (mean: 3 s; max: 39 s). The rule-based heuristic and the robust control approach have the lowest computation times (<30 ms). All four approaches are therefore amenable to implementation.

This paper does not consider the impact of Ground Delay Programs (GDPs). These initiatives are implemented to control the arrival traffic into an airport when the projected traffic demand is expected to exceed the airport's acceptance rate (such as during bad weather). A GDP at a destination airport might result in flights departing from the origin airport to have a delayed take-off time assignment (Expected Departure Clearance Time (EDCT)). One would expect more benefits for flights with EDCT constraints from departure metering because they can have higher gate-holds to meet the EDCT constraint. However, it is worth noting that fewer than on average, fewer than 10% percent of flights experience EDCTs or other related flow constraint (APREQ). A GDP at the origin airport would result in arrivals coming in late, which further impacts the EOBT for the following departures, a factor that is not considered in the current framework. We do, however, consider the impact of bad weather (VMC/IMC) on departure capacity in our queueing models.

VI. Conclusions

This paper presented different departure metering techniques for determining the pushback times to mitigate surface congestion. A trajectory-based optimization approach and three aggregate queue-based approaches were developed and applied to Charlotte Douglas International airport and Charles De Gaulle airport. The departure metering benefits were evaluated using stochastic simulations of the airport surface. The algorithms yield a mean taxi-out time reduction ranging between 1.3 to 2.9 min per flight at CLT. Lower benefits (0.2 to 0.5 min) were observed at CDG since the airport is relatively less congested. Out of the four approaches, the robust control approach that explicitly accounts for model uncertainties performs better in stochastic environments, yielding the highest taxi-out time reduction, while ensuring no adverse impact on the airport throughput.

Acknowledgements

References

[1] Anon., "Comparison of Air Traffic Management-Related Operational Performance: U.S./Europe," https://www.faa.

24

`gov/`, 2015. Retrieved Jan 29, 2019.

[2] Verma, S., Coupe, W. J., Lee, H., Robeson, I., Jung, Y., Sharma, S., Dulchinos, V. L., and Stevens, L., "Tactical Surface Metering Procedures and Information Needs for Charlotte Douglas International Airport," *International Conference on Applied Human Factors and Ergonomics*, Springer, 2018, pp. 157–169. doi:10.1007/978-3-319-93885-1_15.

[3] Simaiakis, I., Khadilkar, H., Balakrishnan, H., Reynolds, T. G., and Hansman, R. J., "Demonstration of reduced airport congestion through pushback rate control," *Transportation Research Part A: Policy and Practice*, Vol. 66, 2014, pp. 251–267. doi:10.1016/j.tra.2014.05.014.

[4] Sharma, S., Capps, A., Engelland, S., and Jung, Y., "Operational Impact of the Baseline Integrated Arrival, Departure, and Surface System Field Demonstration," *2018 IEEE/AIAA 37th Digital Avionics Systems Conference (DASC)*, IEEE, 2018, pp. 1–10. doi:10.1109/DASC.2018.8569828.

[5] Nakahara, A., and Reynolds, T. G., "Estimating current & future system-wide benefits of airport surface congestion management," *10th USA/Europe Air Traffic Management Research and Development Seminar, Chicago*, 2013. Paper ID: 300.

[6] Anon., "Terminal Flight Data Manager Overview," `https://www.faa.gov/air_traffic/technology/tfdm/media/tfdm_overview.pdf`, 2018. Retrieved Aug 23, 2019.

[7] Anon., "Airport CDM implementation manual," `https://www.eurocontrol.int/sites/default/files/publication/files/airport-cdm-manual-2017.PDF`, 2017. Retrieved Aug 23, 2019.

[8] Günther, Y., Inard, A., Werther, B., Bonnier, M., Spies, G., Marsden, A., Temme, M., Böhme, D., Lane, R., and Niederstraßer, H., "Total Airport Management (Operational Concept and Logical Architecture)," `https://elib.dlr.de/45407/1/TAM_OCD_short_v1.0.pdf`, 2006. Retrieved Aug 23, 2019.

[9] Anon., "Changi Airport A-CDM Handbook," `http://changiairport-cdm.sg/`, 2018. Retrieved Dec 12, 2018.

[10] Bosson, C. S., and Sun, D., "Optimization of Airport Surface Operations Under Uncertainty," *Journal of Air Transportation*, Vol. 24, No. 3, 2016, pp. 84–92. doi:10.2514/1.D0013.

[11] Balakrishnan, H., and Jung, Y., "A framework for coordinated surface operations planning at Dallas-Fort Worth International Airport," *AIAA Guidance, Navigation and Control Conference and Exhibit*, 2007. doi:10.2514/6.2007-6553, Paper ID: 2007-6553.

[12] Roling, P. C., and Visser, H. G., "Optimal airport surface traffic planning using mixed-integer linear programming," *International Journal of Aerospace Engineering*, Vol. 2008, No. 1, 2008. doi:10.1155/2008/732828.

[13] Malik, W., Gupta, G., and Jung, Y., "Managing departure aircraft release for efficient airport surface operations," *AIAA Guidance, Navigation, and Control Conference*, 2010. doi:10.2514/6.2010-7696, Paper ID: 2010-7696.

[14] Gotteland, J.-B., Durand, N., Alliot, J.-M., and Page, E., "Aircraft ground traffic optimization," *4th USA/Europe Air Traffic Management Research and Development Seminar, Santa Fe, New Mexico*, 2001. Paper ID= 193.

[15] Deau, R., Gotteland, J.-B., and Durand, N., "Airport surface management and runways scheduling," *8th USA/Europe Air Traffic Management Research and Development Seminar, Napa, California*, 2009. Paper ID = 467.

[16] Ravizza, S., Atkin, J. A., and Burke, E. K., "A more realistic approach for airport ground movement optimisation with stand holding," *Journal of Scheduling*, Vol. 17, No. 5, 2014, pp. 507–520. doi:10.1007/s10951-013-0323-3.

[17] Simaiakis, I., Sandberg, M., and Balakrishnan, H., "Dynamic control of airport departures: Algorithm development and field evaluation," *IEEE Transactions on Intelligent Transportation Systems*, Vol. 15, No. 1, 2014, pp. 285–295. doi: 10.1109/TITS.2013.2278484.

[18] Pujet, N., Delcaire, B., and Feron, E., "Input-output modeling and control of the departure process of busy airports," *Air Traffic Control Quarterly*, Vol. 8, No. 1, 2000, pp. 1–32. doi:10.2514/atcq.8.1.1.

[19] Badrinath, S., and Balakrishnan, H., "Control of a non-stationary tandem queue model of the airport surface," *American Control Conference (ACC)*, IEEE, 2017, pp. 655–661. doi:10.23919/ACC.2017.7963027.

[20] Badrinath, S., Li, M. Z., and Balakrishnan, H., "Integrated Surface–Airspace Model of Airport Departures," *Journal of Guidance, Control, and Dynamics*, Vol. 42, No. 5, 2018, pp. 1049–1063. doi:10.2514/1.G003964.

[21] Anon., "Airport Surface Detection Equipment, Model X (ASDE-X)," https://www.faa.gov, 2018. Retrieved Jan 1, 2019.

[22] Anon., "Aviation System Performance Metrics (ASPM)," http://aspm.faa.gov/, 2018. Retrieved Oct 18, 2018.

[23] Anon., "Airport operations data," https://www.oag.com, 2016. Retrieved Dec 14, 2018.

[24] Anon., "2016 Aircraft Movements," https://aci.aero/data-centre/annual-traffic-data/aircraft-movements/2016-final-summary/, 2016. Retrieved Jan 1, 2018.

[25] Ma, J., Delahaye, D., Sbihi, M., Scala, P., and Mota, M. A. M., "Integrated optimization of terminal maneuvering area and airport at the macroscopic level," *Transportation Research Part C: Emerging Technologies*, Vol. 98, 2019, pp. 338–357. doi:10.1016/j.trc.2018.12.006.

[26] Badrinath, S., Balakrishnan, H., Clemons, E., and Reynolds, T. G., "Evaluating the Impact of Uncertainty on Surface Operations," *2018 Aviation Technology, Integration, and Operations Conference*, AIAA, 2018. doi:10.2514/6.2018-4242.

[27] Badrinath, S., Balakrishnan, H., Clemons, E., and Reynolds, T. G., "Impact of Off-Block Time Uncertainty on the Control of Airport Surface Operations," Transportation Science (in press), 2019.

[28] Slotine, J.-J. E., and Li, W., *Applied nonlinear control*, Prentice hall Englewood Cliffs, NJ, 1991.

[29] Bekiaris-Liberis, N., and Krstic, M., "Compensation of time-varying input and state delays for nonlinear systems," *Journal of Dynamic Systems, Measurement, and Control*, Vol. 134, No. 1, 2012, p. 011009. doi:10.1109/MED.2011.5983098.